Unusual adsorption site of hydrogen on the unreconstructed Ir(100) surface

D. Lerch, A. Klein, A. Schmidt, S. Müller, L. Hammer, and K. Heinz*
Lehrstuhl für Festkörperphysik, Universität Erlangen-Nürnberg, Staudtstrasse 7, D-91058 Erlangen, Germany

M. Weinert
Department of Physics, University of Wisconsin–Milwaukee, P.O. Box 413, Milwaukee, Wisconsin 53201, USA
(Received 22 November 2005; published 23 February 2006)

The adsorption of hydrogen on the metastable, unreconstructed Ir(100)-(1×1) surface is investigated by density functional theory (DFT), quantitative low-energy diffraction (LEED), and thermal desorption spectrometry (TDS) complemented by scanning tunneling microscopy (STM). The bridge site is unequivocally identified as the adsorption site, rather unusual for metallic fcc(100) surfaces. There is excellent quantitative agreement between calculated and experimentally determined structural parameters both for the clean surface and the adsorbate covered surface. Given the uncertainty of DFT to reproduce absolute energies there is also good agreement with the measured adsorption energy (460 meV/atom). Additionally, theoretical vibrational and electronic properties are provided without, however, related experiments being available.

DOI: 10.1103/PhysRevB.73.075430 PACS number(s): 61.14.Hg, 68.43.Bc, 68.43.Fg, 68.43.Vx

I. INTRODUCTION

Hydrogen adsorption on the Ir(100) surface has special consequences when the stable phase of this surface is concerned, i.e., the reconstructed Ir(100)-(5×1) surface whose top layer is quasihexagonally close packed. For high enough temperatures (>180 K) hydrogen adsorption induces this surface to transform to a phase characterized by atomic rows of monatomic width which reside on an unreconstructed (100)-(1×1) substrate.[1] The rows are nearly regularly arranged with an average lateral spacing of $5a$ (with a =2.72 Å the atomic diameter and surface lattice parameter). In order to get a detailed insight into the energetics and structures involved with hydrogen adsorption on Ir we investigated as a first step the adsorption on the unreconstructed surface, Ir(100)-(1×1), a surface which can be prepared as a metastable phase.[2,3]

Moreover, the Ir(100)-(1×1)-H system is interesting with respect to the general systematics characterizing (dissociative) hydrogen adsorption on fcc(100) metal surfaces. For the $3d$-metal Ni, the fourfold hollow site has been determined experimentally.[4] Theory[5–9] found the hollow site to be strongly favored over bridge and top sites by, for monolayer (ML) coverage, 0.193 eV and 0.753 eV per H atom, respectively.[8] In contrast, for the $4d$ metals Pd and Rh the favoring of hollow over bridge sites is (again for 1 ML coverage) only by 0.12 eV (Ref. 10) and 0.085 eV,[11] respectively, while the top site remains very unfavorable, consistent with a recent quantitative low-energy electron diffraction (LEED) investigation of H/Rh(100) that found both hollow and bridge sites occupied, with bridge site occupation increasing with temperature.[12] Within this scenario, the investigation of hydrogen adsorption on a $5d$-metal, here Ir(100), is obviously interesting.

In this paper we investigate the H/Ir(100)-(1×1) system with several theoretical and experimental techniques. On the theoretical side, density functional theory (DFT) is applied to illuminate the energetic, structural, vibrational, and electronic properties of the surface. Also, full dynamical diffraction theory is used to analyze the intensity data collected in the LEED experiments. To explore the energetics of the adsorption experimentally, thermal desorption spectrometry (TDS) was used. The morphology of the surface was imaged by scanning tunneling microscopy (STM) with atomic resolution and the cleanness of the surface was checked by Auger electron spectroscopy (AES).

II. METHODOLOGY

A. Theoretical modeling

1. First-principles calculations

DFT calculations were performed using the projector augmented wave (PAW) method[13,14] of the Vienna *ab initio* simulation package (VASP).[15–17] The exchange correlation was treated within the generalized gradient approximation (GGA) according to Perdew *et al.* (PW91).[18] Application of this functional on bulk iridium results in a lattice parameter a_0=3.878 Å and a bulk modulus B_0=3.40 Mbar which are close to the experimental values (a_0^{exp}=3.839 Å,[19] B_0^{exp} =3.55 Mbar).[20] To examine the influence of the exchange-correlation functional employed, test calculations were performed using the Perdew-Burke-Ernzerhof exchange-correlation functional.[21] Only negligible modifications resulted both for the structure and energetics.

The clean (hydrogen covered) surface was modeled by repeated surface slabs of 9 Ir layers (+H layer) of 17.5 Å thickness (+H layer) separated by a vacuum equivalent to a thickness of 5 Ir layers (9.7 Å). Four Ir atoms per layer were considered to form a $p(2\times2)$ cell in order to allow for a variation of hydrogen coverage (in steps of $\frac{1}{4}$ ML). The slabs were asymmetric in the sense that hydrogen adsorption and multilayer relaxation were considered only on one side. On the other side all four Ir interlayer spacings were kept fixed (bulklike termination). The structural optimization was stopped when the forces computed had decreased below

0.05 eV/Å. Convergence tests showed that lowering the limit to 0.01 eV/Å caused layer spacings to vary by no more than 0.01 Å and the heat of adsorption by no more than 0.1 meV/atom. Brillouin zone sampling used a $(7\times7\times1)$ Monkhorst-Pack mesh consisting of up to 16 irreducible k-points.

To calculate the vibrational frequencies, H atoms were displaced by 0.03 Å with respect to all three coordinates off their ground state positions. The forces acting on the displaced adsorbate atom give them access to the vibration frequency. With 2×2 oscillators per unit cell (equivalent to $\theta_H=1$) Γ-point as well as zone-boundary phonon modes are accessible. Assuming that the adsorbate phonon dispersion is monotonic we approximated the zero-point energy by mean of these values. For $\theta_H<1$ the accuracy for this average is reduced and for $\theta_H=0.25$ even only Γ-point frequencies result. Nevertheless, we are provided with the order of magnitude of the zero-point energy.

In order to rule out significant effects due to the pseudopotential approximation (in particular with respect to the calculation of electronic states), we also applied the full potential linear augmented plane wave (FLAPW) code FLAIR.[22–24] To have comparable results, the PW91-GGA was again used to describe exchange and correlation. This yields a lattice constant of $a_0=3.889$ Å. For the slab calculations a symmetric Ir slab consisting of 13 layers was used, separated by a vacuum of 6 layers thickness. Only a (1×1) unit cell was used, so that only the 1 ML coverage could be tested. On both slab surfaces the five outermost Ir layers and the H layer were relaxed, whereas the central three Ir layers were kept fixed. The Monkhorst-Pack k-point grid was raised to $(18\times18\times2)$ in order to ensure convergence of the electronic band structures of the surface. Both the clean and H covered $(\theta_H=1)$ surface were treated in this way. To compare the results obtained by the FLAPW method and by pseudopotential calculations, the VASP code was also applied to the above described symmetric slab. Only small modifications of interlayer spacings resulted, i.e., 0.02 Å at maximum equivalent to 0.8% for the relative layer relaxations.

2. LEED intensity calculations

The structural evaluation of experimental LEED intensity-vs-energy spectra, $I(E)$, as taken for both the clean and H covered surface requires the dynamical treatment of electron scattering. Such calculations were performed for test model structures using the perturbation method tensor LEED.[25–27] The Erlangen Tensor LEED (TensErLEED) package[28] allows for easy variation of both geometrical and vibrational parameters. Relativistically calculated and spin-averaged phase shifts were used; $l_{\max}=13$ proved to be sufficient for energies up to 600 eV. The attenuation of the electrons by inelastic scattering was simulated by an imaginary part of the inner potential. An energy independent value of $V_{0i}=5.0$ eV reproduced the intensity peak widths excellently. In contrast, the real part of the inner potential, V_{0r}, was allowed to vary with energy because of the large energy range covered and in view of the energy dependence of the exchange correlation potential. According to Ref. 29, the dependence $V_{0r}=V_{00}+\max[-11.48, 0.12-83.64(E/\mathrm{eV}+2.94)^{1/2}]$ eV was applied with the value of V_{00} varied during the course of the theory-experiment fit. The TensErLEED package[28] also contains an automated structural search based on a frustrated simulated annealing procedure[30] guided by the Pendry R factor. The latter's variance, var(R_P), was used to estimate error limits for the parameters determined.[31]

B. Experimental details

The experiments were performed using an ultrahigh vacuum apparatus consisting of two independently pumped vessels. One of them accommodates only a beetle type STM (RHK Technology, Inc.) with the residual gas pressure during operation around 10^{-11} mbar. The other vessel houses backview three-grid LEED optics, a mass spectrometer (VG, SX 200) for TDS, a hemispherical electron analyzer (VG, CLAM 100), and a 5 keV electron gun for AES. Also, there are all tools for sample preparation, positional alignment, and easy transfer between both stages. Due to the extended gas loads required for the preparation of the metastable Ir (100)-(1×1) phase (see below) the background pressure during data acquisition was around 2×10^{-10} mbar. Even this was only feasible by the use of a doser system with the gas inlet realized through a movable nozzle which could be positioned right in front of the sample. This allows an increase in the gas pressure at the surface by 2–3 orders of magnitude compared to the overall pressure in the vessel. By this procedure no quantitative determination of the total exposure to hydrogen was possible.

For the preparation of the metastable (1×1) phase a procedure slightly different from recipes used earlier[2,3,32] was applied: After an initial short sputtering (2 keV Ne^+ ions) the surface was annealed at 1320 K for 3 min. During this time it was dosed with oxygen through the nozzle causing the oxygen partial pressure in the apparatus to increase to 5×10^{-8} mbar. During the subsequent cooling of the sample ($\approx$2 min) and continued dosing by oxygen a (2×1) superstructure was visible in LEED. This state was annealed at 750 K for about 30 s, causing the superstructure spots to disappear. Then, after lowering the temperature to about 550 K, the surface was dosed through the nozzle for 3 min by hydrogen (10^{-8} mbar background pressure). This procedure removes all oxygen from the surface and results in a sharp and low-background (1×1) LEED pattern. Due to the very good orientation of the surface (better than 0.1°), very large and flat domains with widths of several thousand Ångstrøms appeared in the STM. A large scale image exhibiting a single terrace is displayed in Fig. 1 with an atomically resolved image inserted.

The surface morphology resulting from the above described preparation procedure contrasts to that obtained by our earlier preparation method[32] where mostly square (1×1) islands residing on the unreconstructed substrate were found. These islands seem to nucleate from atoms expelled from the hexagonal overlayer during the lifting of the reconstruction. In the present case it appears that there is enhanced diffusion of the atoms expelled so that, in spite of the large terrace widths, they can arrive at and coordinate step edges (step flow growth). As evident from Fig. 1, there

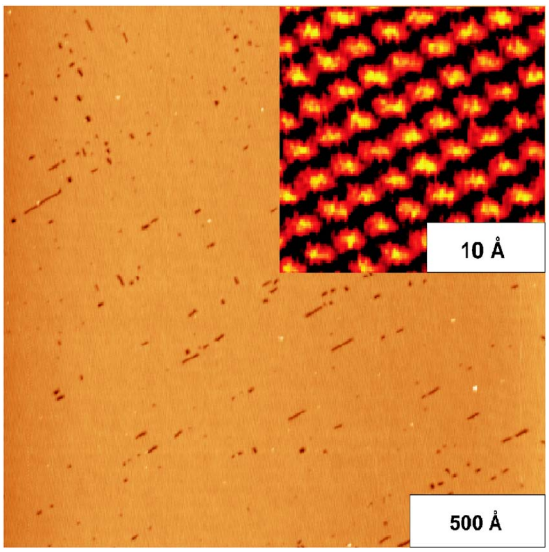

FIG. 1. (Color online) Large scale STM image (2000 Å $\times$2000 Å, U_{tip}=−1.00 V, I=3.33 nA) of the metastable Ir(100)-(1$\times$1) phase with a zoom to atomic resolution inserted (U_{tip} =−2.75 mV, I=10.1 nA).

are statistically distributed (and sometimes extended) holes on the unreconstructed terrace. Their diffusion is inhibited as might be the case for impurities. Yet, as there is no indication of impurities by AES, we tend to attribute the feature to the additional extraction of atoms from the former hexagonal layer and to some limited diffusion of the holes created this way.

Adsorption of hydrogen on Ir(100)-(1$\times$1) did not lead to any superstructure, irrespective of the total exposure and the adsorption temperature. In addition, LEED intensity-vs-energy spectra, $I(E)$, changed only very slightly, indicative of only small structural modifications induced by the adsorbate.

The $I(E)$ curves were taken at normal incidence of the primary beam for both the clean and hydrogen saturated surface. For the measurement of the clean surface the sample was kept at about 470 K which is above the desorption temperature of hydrogen (see below). This was done in order to avoid hydrogen adsorption from the residual gas which consists mainly of hydrogen due to the preparation procedure described. In contrast, the H-saturated (1$\times$1) surface was prepared by hydrogen dosing through the nozzle at room temperature (estimated exposure of several 100 L). Subsequently, the sample was cooled to about 100 K for the intensity measurements in order to reduce thermal diffuse scattering and to increase the possibility of detecting hydrogen in the intensity analysis despite its low scattering strength. A charge coupled device (CCD) video camera operated under computer control was used to store full diffraction images on a hard disk in steps of 0.5 eV between 50 and 600 eV primary beam energy allowing for total measuring times of about 15 min. The intensity spectra of individual beams resulted from off-line evaluation as described in detail earlier.[27,33] Symmetrically equivalent beams were averaged as usual. The energy width of all accumulated inequivalent beams amounts to ΔE=2255 eV for the clean surface and ΔE=2290 eV for the H-covered phase.

TABLE I. Comparison of spacings $d_{i,i+1}$ between layers i and $i+1$ and their relative deviations from the bulk value d_b for clean Ir(100)-(1$\times$1) as resulting by DFT and quantitative LEED. The LEED results are given with 0.01 Å [0.5%], those of DFT with about 0.004 Å [0.2%] accuracy.

	DFT (VASP)	LEED
d_b (Å)	1.939	1.924
d_{12}(Å)[$(d_{12}-d_b)/d_b$(%)]	1.834 [−5.4]	1.84 [−4.5]
d_{23}(Å)[$(d_{23}-d_b)/d_b$(%)]	1.961 [+1.1]	1.93 [+0.5]
d_{34}(Å)[$(d_{34}-d_b)/d_b$(%)]	1.951 [+0.6]	1.93 [+0.5]
d_{45}(Å)[$(d_{45}-d_b)/d_b$(%)]	1.940 [+0.1]	1.92 [±0.0]
d_{56}(Å)[$(d_{56}-d_b)/d_b$(%)]	1.942 [+0.1]	1.93 [+0.5]

The energetics of the hydrogen adsorption was investigated by TDS. After (dissociative) adsorption of hydrogen the temperature of the sample was raised linearly with time (1 K/s). The desorbing hydrogen was measured by a quadrupole mass spectrometer, whose complete housing with an entrance smaller than the sample diameter and its location right in front of the sample prevents significant contributions from desorption from the sample holder. In addition, because there is a separate pumping line into the main pump there was only little increase of the background signal during a desorption sweep. So, the actual pressure in the mass spectrometer is proportional to the desorption rate.

III. STRUCTURE OF CLEAN Ir(100)-(1×1)

The clean Ir(100)-(1$\times$1) surface is a good test case for the agreement between our first-principles calculations and experiment, here DFT and LEED. Though the surface structure has been determined by quantitative LEED earlier,[32,34] we repeated the analysis for the very sample used and extended it to the variation of the top five interlayer spacings. Also, vibrational amplitudes in the first and second layer were allowed to vary from the value common for all layers below. This is of importance because of the rather high temperature of measurement. Note that in spite of the high temperature of measurement, the thermal expansion is very small (about 0.3% compared to zero temperature), so that comparison to the results by DFT (which neglects any lattice vibrations) can be made. The relaxation profile determined is typical for metallic fcc(100) surfaces: A top spacing contraction is followed by an expansion and the spacings relax quickly to the bulk value when going deeper into the surface. Deviations of deeper spacing from d_b are within the limits of errors.

The LEED fit produced a very good level of theory-experiment agreement equivalent to a Pendry R-factor of R_P=0.11. Within 0.01 Å—which is also the order of magnitude of the statistical error as estimated by the R-factor variance[31]—the interlayer spacings are the same as in our earlier analysis.[32] Table I provides the DFT-LEED comparison both for the absolute spacings and their relative changes with respect to the bulk value. The latter values are more relevant as the lattice parameter produced by the DFT

slightly deviates from the experimental value. Evidently, the agreement between theory and experiment is excellent, the relative values differ by less than 1%, about the value of the error limits involved. This is a promising starting point for the treatment of the hydrogen adsorption system.

IV. RESULTS FOR HYDROGEN COVERED Ir(100)-(1×1)

In the study of hydrogen adsorption on Ir(100)-(1×1) we concentrated mainly on two aspects: First, we investigated the energetics for different adsorption sites as well as for varying coverage in order to get information on the relative stability of the different adsorbate structures as function of coverage. Our second, though not independent, focus is the crystallography of the structures, i.e., the adsorption height in a certain site *and* the structural changes hydrogen induces within the substrate. To the first question and with respect to the comparison of different sites only the DFT has access, but DFT and TDS should agree for the energetics of the equilibrium phase assumed in experiment. Similarly, DFT and LEED should give the same result for the crystallographic parameters of this phase.

Last but not least, DFT gives access to vibrational and electronic properties of the adsorbate system; these are presented here even though experimental verification is lacking (but which is encouraged with this paper).

A. Energetics

1. First-principles calculations

For the adsorption of H on the Ir(100)-(1×1) surface we studied the different phases in the coverage range 0–1 ML in steps of 1/4 ML allowing for single site occupation of hollow, bridge, and top positions by hydrogen as illustrated in Fig. 2. As there are two bridge sites per (1×1) unit cell (twice as many as hollow and top positions) the maximum coverage to be investigated is $\Theta_H=2$. Also, for $\Theta_H=1/2$ there are two inequivalent (2×1) superstructures. In phase *A* half of the top-layer Ir atoms are twofold coordinated to H atoms and the other half remains uncoordinated, while in phase *B* there is single H coordination for all Ir atoms. In addition to the phases displayed in Fig. 2, we checked also for subsurface hydrogen, only for $\theta_H=1$, and allowing for octahedron and tetrahedron sites just below the first Ir layer. These latter efforts were undertaken just for completeness in spite of the fact that no experimental indications exist for subsurface hydrogen.

A useful quantity for the treatment of the adsorption system is the heat of adsorption as defined by

$$E_{ad} = -\frac{1}{n}\left(E_{Ir+nH} - E_{Ir} - \frac{n}{2}E_{H_2}\right), \tag{1}$$

which provides the energy gain per adsorbate atom relative to the energy in the gas phase. E_{Ir+nH} denotes the total electronic energy of the substrate slab covered by n adsorbate atoms in the assumed (2×2) unit cell, E_{Ir} is that of the clean substrate slab and E_{H_2} that of the free hydrogen molecule. As defined with a negative sign, the ground state corresponds to the adsorption site which yields the highest (positive) value of E_{ad}. Sites with negative heat of adsorption are unstable.

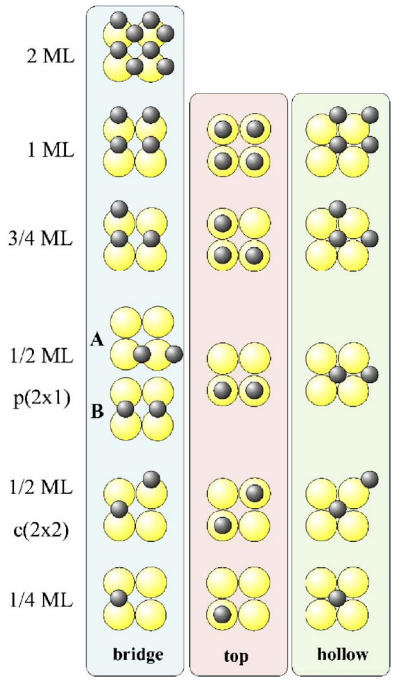

FIG. 2. (Color online) Top view of the adsorbate configurations tested.

The above definition of E_{ad} considers only the adsorption potential for the hydrogen atom, but neglects the vibrational ground state energy of hydrogen, which is significant for chemisorbed light atoms. To correct it, we average over the $3n$ vibrational modes ω_i resulting in

$$E_{H_{ad}}^{vib} = \frac{1}{n}\sum_{i=1}^{3n}\frac{1}{2}\hbar\omega_i. \tag{2}$$

From this we have to subtract the vibrational ground state energy of the free molecule ($\hbar\omega_{H_2}/2=264$ meV) which has not been considered so far, too, so that the total vibrational correction per atom reads as

$$\Delta E^{vib} = E_{H_{ad}}^{vib} - \tfrac{1}{2}\tfrac{1}{2}\hbar\omega_{H_2} \tag{3}$$

leading to the zero-point vibration corrected form of the heat of adsorption

$$E_{ad}^{cor} = E_{ad} - \Delta E^{vib}. \tag{4}$$

Table II provides the results for E_{ad}, E_{ad}^{cor}, and $E_{H_{ad}}^{vib}$ for the five coverage values and the various adsorption sites assumed. Surprisingly, the bridge site is the favored adsorption site in the entire coverage regime. Compared to the hollow site, which is generally expected to be the favored site on fcc(100) metal surfaces, the coverage averaged energy difference is as high as 320 meV. Even the top site (120 meV below bridge site) appears to be less unfavorable. These rather large energy differences are responsible for the result that the relative stability of the various adsorption phases

TABLE II. DFT results for all investigated configurations of hydrogen on of Ir(100)-(1×1), i.e., as function of coverage for bridge (bri), top (top), hollow (hol), subsurface octahedron (oct), and tetrahedron (tet) sites. The numbers in italics in the last row correspond to the stable phases. For the definition of the different energies see text.

θ_H (ML)	Sites/order	E_{ad} (meV)	$E_{H_{ad}}^{vib}$ (meV)	$E_{\mathrm{ad}}^{\mathrm{cor}}$ (meV)
2	bri $c(1\times1)$	496	205	***423***
1	bri $p(1\times1)$	705	177	***661***
	top $p(1\times1)$	552	184	**501**
	hol $p(1\times1)$	290	114	**308**
1	oct $p(1\times1)$	−1056	not calc.	not calc.
(subsurf.)	tet $p(1\times1)$	−1096	not calc.	not calc.
$\frac{3}{4}$	bri $p(2\times2)$	696	174	***654***
	top $p(2\times2)$	561	180	**513**
	hol $p(2\times2)$	308	120	**320**
$\frac{1}{2}$	bri $p(2\times1)$A	696	169	***659***
	bri $p(2\times1)$B	690	176	**646**
	bri $c(2\times2)$	673	171	**634**
	top $c(2\times2)$	611	177	**566**
	top $p(2\times1)$	557	177	**512**
	hol $p(2\times1)$	329	119	**342**
	hol $c(2\times2)$	319	133	**318**
$\frac{1}{4}$	bri $p(2\times2)$	677	168	***641***
	top $p(2\times2)$	592	174	**550**
	hol $p(2\times2)$	345	125	**352**

remains qualitatively unchanged even though the vibrational ground state energies for the different adsorption sites vary by up to 70 meV.

Both subsurface sites are unstable by more than 1 eV with respect to the gas phase at $\theta_H=1$. Therefore, they were not taken into consideration for $\theta_H<1$. Also, because of the strong preference of bridge sites in the entire coverage regime, mixed site occupations (e.g., 0.5 ML on bridge and 0.5 ML on top sites) were not tested as they appear highly improbable on the basis of the present results.

The coverage dependency of the heat of adsorption as displayed in Fig. 3 gives some insight into the interactions between adsorbate atoms. As the atomic radius of H is considerably smaller than the Ir nearest-neighbor distance (2.7 Å) the interaction is most likely a multiparticle interaction mediated through the substrate. For the least stable adsorption site, the hollow site, E_{ad}^{cor} exhibits a monotonic decrease with increasing coverage, i.e., the adsorption of more hydrogen becomes less and less favorable by geometric and/or electronic modifications induced on the substrate. Yet, this feature is only of academic interest as hollow site adsorption cannot be expected to be realized in experiment due to the comparably low heat of adsorption. The same holds for top site adsorption.

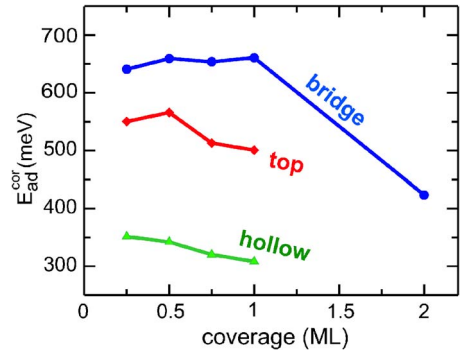

FIG. 3. (Color online) Coverage dependence of the zero-point corrected heat of adsorption (E_{ad}^{cor}) for different adsorption sites as calculated by the DFT.

The only coverage dependency amenable to experimental verification is that of bridge site adsorption. In the submonolayer regime we find a slight increase in the calculated heat of adsorption with coverage up to the most stable phase at $\theta_H=1$ at which $E_{ad}^{cor}=661$ meV. Energy is also gained when a second layer of hydrogen is adsorbed in the second bridge site, at $\theta_H=2$. The calculation of the heat of adsorption for the second bridge site only (with the first already occupied) yields a value as small as 185 meV which makes adsorption at room temperature improbable. The variation of E_{ad}^{cor} with coverage in the submonolayer regime is only by 27 meV (at most) and might be within the limits of errors (see below). In any case, it should have, at least at elevated temperatures, no effect with respect to some possible clustering to patches of 1 ML local coverage. It is also in line with our observation that there are no adsorption superstructures appearing in LEED, neither at room temperature nor at the temperature of intensity data acquisition (≈100 K).

By symmetry arguments, only the $p(2\times1)$, $p(2\times2)$, and $c(2\times2)$ phases allow for some adsorbate induced atomic buckling within the substrate. Yet, the corresponding movements of Ir atoms are all rather small, in any case smaller or even much smaller than 0.05 Å. In view of this weak effect and the expectation that only the (1×1) phase is experimentally realized, we do not consider this feature further.

At this point we need to address the reliability of our DFT results in view of the well known fact that DFT calculations often fail to reproduce *absolute* energies accurately. Though, in comparison to the local density approximation (LDA), GGA's like PW91 lead to more reliable energies,[18,35] they can also produce a considerable overbinding[36] as has been found in various studies of adsorption energies (e.g., Refs. 37 and 38). Therefore, further developed GGA's have been proposed to improve this situation, in particular by proposals of Perdew, Burke, and Ernzerhof[21] (PBE) and revised versions of that as proposed by Zhang and Young[39] (revPBE) or, subsequently, by Hammer, Hansen, and Nørskov[38] (RPBE). Both revPBE and RPBE, which adapt the gradient correction to molecular and adsorptive binding, were reported to produce adsorption energies much closer to experimental values than PW91 and PBE (our test calculations using the latter two GGA's produced only small modifications). For oxygen adsorbed in fcc hollow sites on Ni(111) the use of revPBE

produces an adsorption energy of 4.83 eV (close to the experimental value of 4.84 eV) while the values yielded by PBE (5.27 eV) and PW91 (5.38 eV) are much worse.[38] Though for a more weakly bound adsorbate (as hydrogen in our case) the effect should not be as large, caution has to be played.

We therefore tried to estimate the errors within the framework of our present calculations. As obvious from Eqs. (1)–(4), the total electronic energy of the free H_2 molecule, E_{H_2}, as well as its zero-point vibrational energy (frequency ω_{H_2}) are subtracted in the calculation of the absolute values for the hydrogen adsorption energies. So, the precision with which the absolute values of the latter can be calculated depends critically on the precision for E_{H_2} and ω_{H_2}. For the frequency we calculated $\omega_{H_2}^{calc}=4260\ \mathrm{cm}^{-1}$ which, as typical for gradient-corrected calculations, is somewhat underestimated and so lower than the experimental value, $\omega_{H_2}^{\mathrm{exp}}=4400\ \mathrm{cm}^{-1}$.[40] Unfortunately, for the total energy E_{H_2} the use of pseudopotentials results in a physically meaningless value. However, by additionally and in the same way computing the total energy of the H atom, E_H, one can calculate the binding energy of the H_2 molecule, $E_{B,H_2}=E_{H_2}-2E_H$. The resulting value, $E_{B,H_2}^{calc}=4.53$ eV is close to the results of comparable theoretical studies (e.g., Refs. 8 and 11). Yet, after zero-point correction (132 meV/atom) it results to be significantly lower (4.27 eV) than the experimental value, $E_{B,H_2}^{\mathrm{exp}}=4.478$ eV.[40] Clearly, this must lead to an equally incorrect *absolute* value for the heat of adsorption which must be expected to be (per atom adsorbed) of the order of 0.1 eV higher than the experimental value (therefore, not rarely the experimental value for E_{B,H_2}^{exp} has been used within theoretical calculations for hydrogen adsorption energies, e.g., Refs. 10 and 41). One may assume that the error in calculating $(1/n)\times E_{Ir+nH}$ in Eq. (1) is of similar magnitude, so that the total error may amount to about 0.2 eV.

Fortunately, however, the consequences should be much less serious when *differences* between the adsorption energies of different sites are considered. So, the error for E_{H_2} discussed above cancels completely. Assuming that the error involved in the calculation of E_{Ir+nH} is largely independent of the adsorption site, the predicted hierarchy of sites with respect to energy should be rather accurate. This is consistent with a comparison we made for absolute energies obtained by VASP and FLAIR (for the modified set up described in Sec. II A). It appears that, for the adsorption sites investigated, VASP gives *always a smaller* heat of adsorption and the differences are rather small, i.e., 41 meV for hollow, 32 meV for bridge, and 11 meV for top position. As a consequence and due to the large energy differences obtained for different sites at a certain coverage (e.g., >160 meV for $\theta_H=1$) the energetic hierarchy of adsorption sites remains the same.

2. Experimental determination by TDS

In the value of the heat of adsorption calculated above no activation energy for the dissociation of the hydrogen molecule enters, only equilibrium energies. Therefore, E_{ad}^{cor} can only be accessed by TDS when no such activation energy exists, so that E_{des} is directly related to E_{ad}^{cor}. Assuming this case holds, we recorded desorption spectra by applying a temperature increasing linearly with time and evaluated them to yield E_{des} experimentally. The mass spectrometer measured hydrogen molecules rather than atoms and, consistently, the spectra [a selection of which is shown in Fig. 4(a)] clearly exhibit second order, i.e., recombinative desorption.

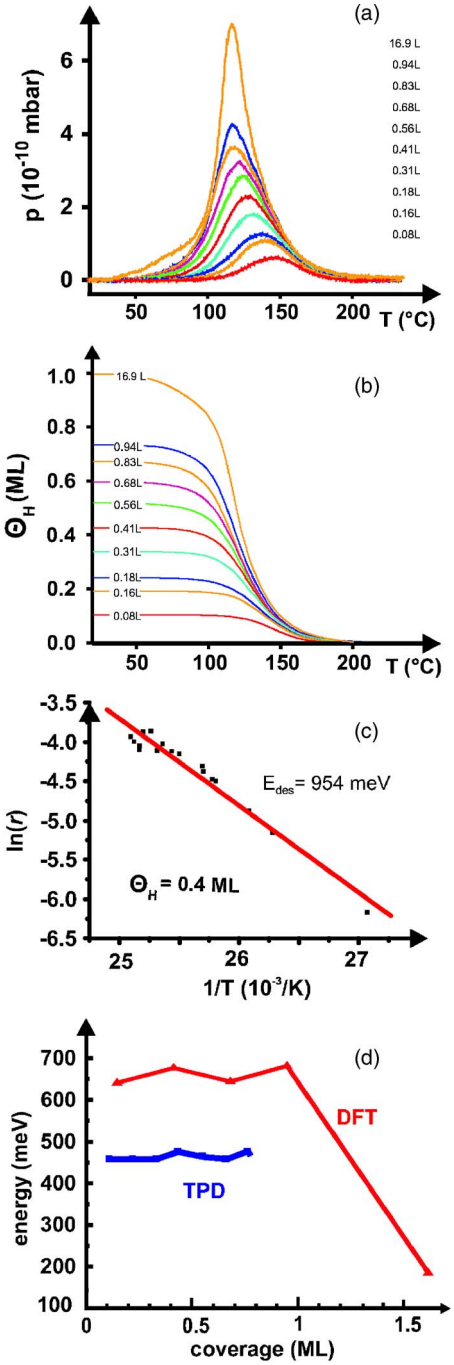

FIG. 4. (Color online) Selection of measured (a) and integrated (b) TPD spectra and evaluation for a certain coverage (c). In panel (d) the desorption energies per hydrogen atom as resulting from TPD measurements, $\frac{1}{2}E_{des}(\theta_H)$, are compared to those calculated from the DFT results by $\tilde{E}_{ad}(\theta_H)=E_{ad}^{cor}(\theta_H)+\theta_H\Delta E_{ad}^{cor}/\Delta\theta_H$ (see text).

This is both by the (nearly) symmetric shape of peaks[42] and by the shift of peak maxima to lower temperatures with increasing coverage. The latter feature also shows that there is no clustering to patches of local full monolayer coverage (in particular at the elevated temperatures involved in the desorption process) because in this case the local coverage would always be the same, so that no peak shifts to lower temperatures would result. As a consequence of the recombinative desorption we measure the desorption energy of the hydrogen molecule, i.e., $\frac{1}{2}E_{des}$ accounts per hydrogen atom. Evaluation of the data to extract E_{des} was made following the procedure proposed by King *et al.*[43,44] This starts from the Wigner-Polanyi equation for the desorption rate $r(T)$

$$-d\theta_H/dt(T) \equiv r(T) = \nu(\theta_H)^n \exp[-E_{des}(\theta_H)/kT] \qquad (5)$$

whereby n denotes the order of desorption and ν the (unknown) attempt frequency for desorption. Corresponding spectra for different initial coverage values θ_0 are displayed in Fig. 4(a). Taking the logarithm results in

$$\ln[r(T)] = \ln(\nu) + n\ln(\theta_H) - E_{des}(\theta_H)/kT. \qquad (6)$$

Evidently, the dependence $E_{des}(\theta_H)$ can be retrieved—independent of the precise knowledge of n and $\nu = \nu(\theta_H)$—by plotting the desorption rate as function of $1/T$ (Arrhenius plot). Yet, as θ_H is the instantaneous coverage which varies during the desorption process, a more complex data evaluation is necessary to yield $E_{des}(\theta_H)$. Each of the spectra in Fig. 4(a) is integrated to yield $\theta_H(T,\theta_H^0) = \int_T^\infty r(T',\theta_H^0)dT'$ providing, for $T \to 0$, also the total initial coverage θ_H^0 in each case as illustrated in Fig. 4(b) [the highest achievable coverage (saturation) was identified with $\theta_H^0 = 1$, an assumption which is corroborated by the LEED results, see below]. The corresponding set of curves allows for a chosen constant coverage [a horizontal line in Fig. 4(b)] to identify a set of temperatures and—via correlation to the original spectra in Fig. 4(a)—the corresponding set of desorption rates. So, an Arrhenius plot can be constructed for constant coverage [as displayed in Fig. 4(c)] from whose slope $E_{des}(\theta_H)$ can be taken.

This procedure is repeated for different values of θ_H and the resulting values for $\frac{1}{2}E_{des}(\theta_H)$ are displayed in Fig. 4(d). For comparison with the coverage dependent binding energies calculated by DFT in Sec. IV A 1 one has to consider that the latter refer to the average per atom while the desorption energy refers to atoms desorbed *at* a certain coverage. As a consequence comparison of $\frac{1}{2}E_{des}(\theta_H^0)$ should be made to $\tilde{E}_{ad}(\theta_H) = E_{ad}^{cor}(\theta_H) + \theta_H \Delta E_{ad}^{cor}/\Delta\theta_H$ and these values are plotted in Fig. 4(d).

As obvious from Fig. 4(d) the experimental energy values are lower than the theoretical ones, whereby the average deviation is about 0.2 eV. This is the order of the systematic shift we have estimated for our DFT calculations, so the theory-experiment agreement appears to be reasonable.

B. Structure

As described above, the first-principles calculations strongly favor bridge-site occupation. The minimization procedure of interatomic forces to find the maximum heat of adsorption provides, of course, also the related crystallographic structure. Table III presents the corresponding structural parameters for monolayer coverage, i.e., the hydrogen adsorption height in the bridge site as well as the related interlayer spacings in the substrate.

TABLE III. Structural details of the H covered surface as predicted by DFT (1 ML H on bridge sites) and determined by quantitative LEED structure analysis ($R_P = 0.101$).

	DFT (VASP)	LEED
d_H (Å)	1.178	1.23
d_{12}(Å)[$\Delta d_{12}/d_b$(%)]	1.874 [−3.3]	1.86 [−3.1]
d_{23}(Å)[$\Delta d_{23}/d_b$(%)]	1.950 [+0.6]	1.93 [+0.5]
d_{34}(Å)[$\Delta d_{34}/d_b$(%)]	1.945 [+0.3]	1.93 [+0.5]
d_{45}(Å)[$\Delta d_{45}/d_b$(%)]	1.931 [−0.4]	1.91 [−0.5]
d_{56}(Å)[$\Delta d_{56}/d_b$(%)]	1.939 [±0.0]	1.92 [±0.0]

Corroboration of the structural DFT result by quantitative LEED is not an easy task for the present case. The method frequently has proved to reliably determine structures with an accuracy in the picometer range.[45] Yet, for hydrogen adsorbates the positions of the adatoms are much less certain. This is because of hydrogen's low scattering strength compared to that of substrate atoms in particular in the present case with a scatterer as strong as Ir involved. For complex substrate structures (with many structural parameters) there is frequently no chance at all to determine the position(s) of the hydrogen atom(s).[46] Fortunately, for a substrate structure as simple as in the present case [(1×1) phase with only a few interlayer spacings as parameters] there is a good chance to detect hydrogen though its resulting positional parameters must be expected to be about an order of magnitude less accurate than those of substrate atoms.[46] Even more, the (small) structural modifications of the substrate induced by hydrogen should depend on the latter's adsorption geometry so that the substrate structure is kind of a fingerprint for the adsorption site. As LEED resolves this with high accuracy there is an additional chance to identify the correct adsorption site of hydrogen by comparison to the DFT results for the substrate structure.

Assuming the surface to be covered by 1 ML of hydrogen the best fit Pendry R factors resulting for bridge, hollow, and top sites are $R_P = 0.101$, 0.148, and 0.144, respectively. So, with an R-factor variance of $\mathrm{var}(R) \approx 0.01$ nonbridge sites can be excluded. Also, the 2 ML phase with two bridge sites per Ir atom occupied is unlikely by its R-factor $R_P = 0.120$. Neglecting hydrogen scattering in the analysis, i.e., assuming zero or negligible coverage, leads to $R_P = 0.111$. This favors in fact full monolayer coverage (with hydrogen in bridge sites). We will return to this point in more detail below.

Table III displays the structural results for the best fit, i.e., bridge position of the adsorbates. Given the relatively large uncertainty (±0.1 Å) due to hydrogen's weak scattering, the adsorption height is close to the DFT value. Yet, even more convincing for the comparison of the LEED and DFT results are, because of the high LEED precision involved, the sub-

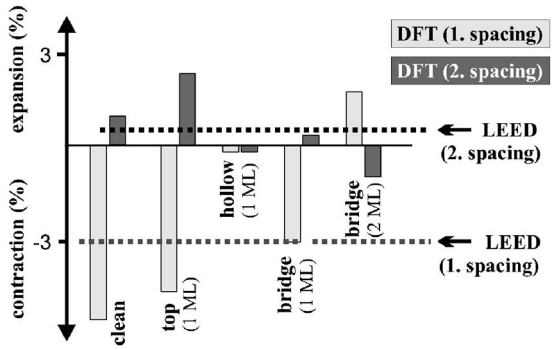

FIG. 5. Relative interlayer relaxations calculated by DFT for the different adsorption geometries (and the clean surface) as compared to the LEED result.

strate interlayer spacings which are numerically given in Table III for the bridge site and in a graphic overview for all sites investigated (as well as for the clean surface) in Fig. 5. As discussed above, the calculated substrate relaxation profile changes significantly with the adsorption site, i.e., it can be taken as a fingerprint for these sites. Only for the bridge site do DFT and quantitative LEED agree, whereby the relative relaxations differ by not more than 0.2%.

As pointed out above we have assumed full monolayer coverage (as saturation coverage) both for the evaluation of the TDS data and the LEED intensity analysis. This assumption can be confirmed again by exploiting the fingerprint property of the substrate structure, i.e., by comparing the hydrogen induced substrate relaxations calculated for varying coverage with the LEED result. Figure 6 displays this coverage dependence for the relaxation of the top layer spacing which is most sensitive to adsorption (in case of adsorbate induced bucklings in the substrate the average layer spacing is considered). There is a clear coverage dependence of the relaxation which is practically linear (at least in the beginning) as has been also quantitatively determined for hydrogen adsorption on Rh(110).[47] The experimental value is only met at full monolayer coverage, so confirming the above assumption. The LEED result for the substrate relaxations is largely independent of whether or not hydrogen scattering is considered in the intensity analysis and in which adsorption site. Thus, the identification of full coverage as demonstrated in Fig. 6 is even possible without knowledge of the hydrogen adsorption structure.

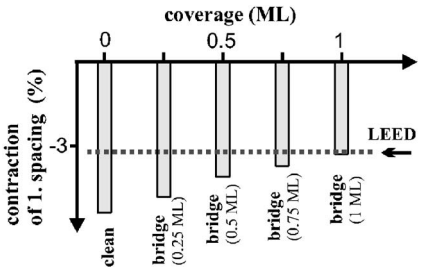

FIG. 6. Contraction of the top layer spacing for bridge site occupation as function of coverage as calculated by DFT (columns). Comparison to the experimental LEED result for coverage saturation (broken line).

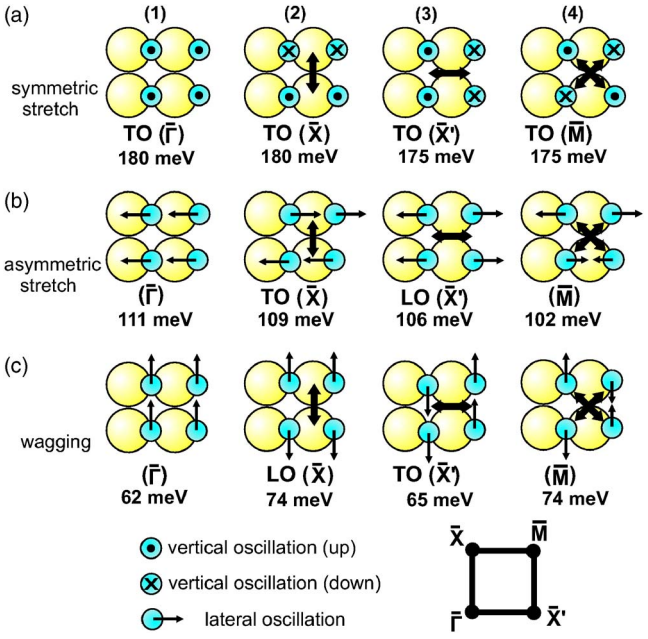

FIG. 7. (Color online) DFT-calculated energies of hydrogen vibration modes as indicated. Bold arrows in panels denote the direction of the wave vectors involved in correspondence to the irreducible surface Brillouin zone (boundary) points displayed on the lower right.

C. Vibrational properties

The vibronic properties of hydrogen adsorbed on surfaces have been frequently investigated experimentally and theoretically, in particular because of their relevance for dynamical processes as diffusion and reactions as well as quantum delocalization in excited vibronic states (for a recent review see Ref. 48). The vibrational energies found on transition metals are typically in the range 60–160 meV and the activation energy for diffusion at about 200 meV.[48] So, for the hollow site adsorption on Ni(100) a symmetric stretch-mode energy of 80 meV was found by electron energy loss spectroscopy (EELS) as well as an asymmetric stretch mode which disperses from about 87 meV at the $\bar{\Gamma}$-point to 105 meV at the $\bar{X}$-point.[49]

As the present paper reports on bridge-site occupation on an fcc(100) surface for the first time we provide the reader also with calculated vibrational energies, though no corresponding experimental data seem to exist. We must expect that the force constants for displacements of the different hydrogen atoms in the (2×2) unit cell off their equilibrium positions depend on the vibrational mode, i.e., the relation between the different displacements. Accordingly, we calculated the energies of the related vibration modes as indicated in Figs. 7(a)–7(c) for the full monolayer case, i.e., the situation met in experiment.

The symmetric stretch modes shown in row (a) of Fig. 7 are for vertical displacements of the adatoms and are of transverse optical (TO) character as neighboring atomic rows are displaced antiphase-like (except for the $\bar{\Gamma}$-point). As only a (2×2) superstructure is considered the corresponding reciprocal space points, which the calculations can provide, are

at the boundaries of the surface Brillouin zone as indicated on the lower right of Fig. 7. The panels displayed in rows (b) and (c) show the modes for the two in-plane polarizations of the vibrations, i.e., the asymmetric stretch and the wagging modes. In all cases the $\bar{\Gamma}$-point energy and the energy at the boundary are rather similar which we interpret to be indicative (though not fully conclusive) for only weak dispersion of the modes. Intuitively understandable is the fact that the modes with polarization vertical to the surface are of higher energy than the modes with in-plane polarization. The same holds for comparing the subcases of the latter: modes with vibration amplitudes towards the hollow site are of lower energy than the modes with amplitudes towards atomic top sites. It appears that the symmetric stretch-mode energies fall slightly above the range of energies mentioned above, whereby all other energies are well within it.

D. Electronic properties

There are a number of surface states and resonances on the clean Ir(100) surface [Fig. 8(a)]. The modification of these states with the adsorption of hydrogen depends on the adsorption site. Thus, measurement of the photoemission and inverse photoemission spectra can provide further, albeit indirect experimental evidence of hydrogen adsorption site.

The distingushing feature for the hollow site [Fig. 8(c)] is a strong surface state split off below the bands along $\bar{\Gamma}$-$\bar{M}$ ($\bar{\Sigma}$), especially around $\bar{M}$; none of the other sites has this state. For the top site [Fig. 8(d)], there is a flat surface resonance at ~ -5 eV centered around $\bar{\Gamma}$ and extending at least a quarter of the way to the zone boundaries along both $\bar{\Sigma}$ and $\bar{\Delta}$ ($\bar{\Gamma}$-$\bar{X}$).

The bridge site [Fig. 8(b)] also has a surface feature around $\bar{\Gamma}$, but nearer to the Fermi level (~ -3.8 eV) and existing only very close to $\bar{\Gamma}$. The surface states found in both the occupied and unoccupied bulk gaps around $\bar{X}$ provide the best identification: There are two states in the unoccupied gap, one near the bottom (also seen for the clean surface, and for the top and hollow sites) and a second one near the top of the gap that is seen only for the bridge site. The state in the gap below the Fermi level starts at $\bar{X}$ and increases in localization until it crosses the bulk bands. In addition, there is a surface resonance dispersing slightly downward below the bottom of the gap. Although there are also surface states for the hollow and top sites in this gap, there are distinct differences: for the top site the state follows the top of the gap, while for the hollow site the state disperses quickly upward; in both cases the second resonance is missing.

V. DISCUSSION AND CONCLUSION

Our investigations have unequivocally revealed that the bridge site is the energetically favored hydrogen adsorption position on Ir(100)-(1×1). We know of no other fcc(100) metal surface for which this has been detected as the stable site either by theoretical or by experimental investigations. Instead, the three quantitatively investigated fcc(100) sur-

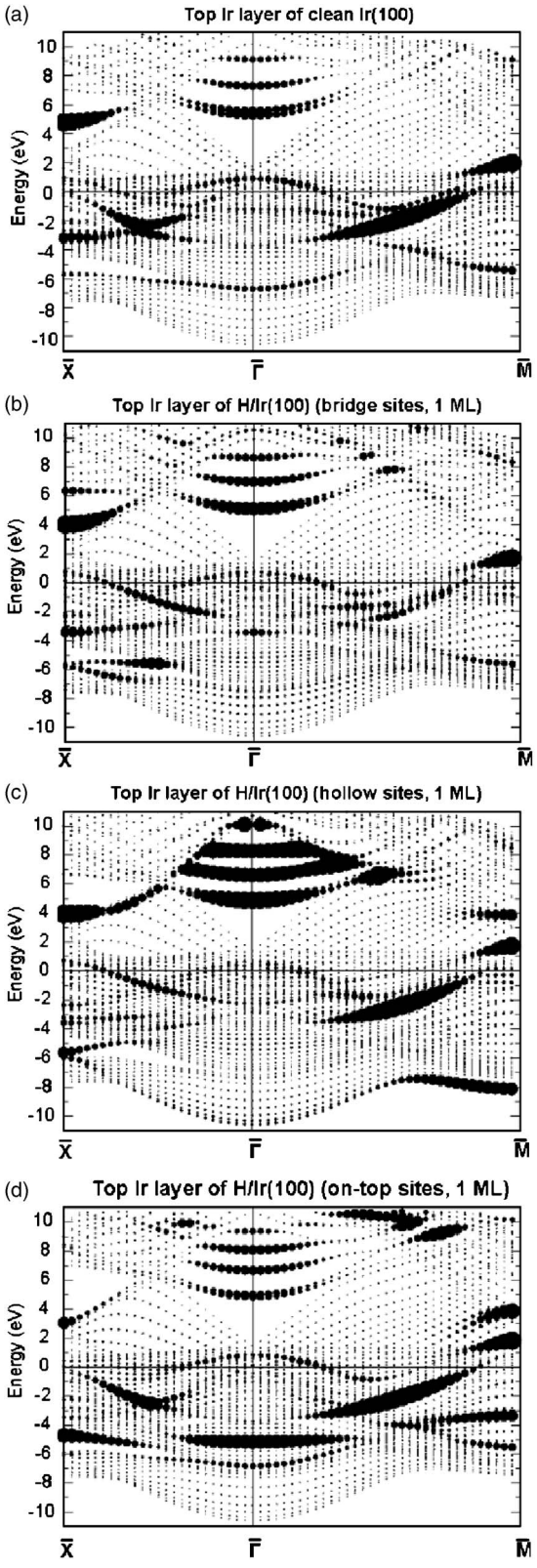

FIG. 8. Calculated band structure for (a) the clean Ir(100)-(1×1) surface and the (1×1) hydrogen-covered surface with 1 ML H adsorbed at the bridge (b), hollow (c), and top (d) sites. The radii of the circles are proportional to the relative weight of the state in the top Ir (and adsorbate) layer.

TABLE IV. Comparison of calculated and measured hydrogen adsorption energies and covalent radii as far as available for the (100) surface of Ni, Rh, and Pd with the corresponding parameters of the present investigation for H/Ir(100).

	Ni(100)	Rh(100)	Pd(100)	Ir(100) [this work]
E_{bri}^{calc} (meV)	391 (Ref. 8)	483 (Ref. 11)	315 (Ref. 10)	**661**
	390 (Ref. 9)	410 (Ref. 10)	400 (Ref. 50)	
E_{hol}^{calc} (meV)	**584** (Ref. 8)	**568** (Ref. 11)	**435** (Ref. 10)	308
	546 (Ref. 9)	**450** (Ref. 10)	**520** (Ref. 50)	
E_{top}^{calc} (meV)	−169 (Ref. 8)	50 (Ref. 10)	−80 (Ref. 50)	501
	−61 (Ref. 9)		165 (Ref. 10)	
E^{exp} (meV)	499 (Ref. 51)	520 (Ref. 52)	530 (Ref. 53)	460
r_H^{calc} (Å)	0.57 (Ref. 8)	0.63 (Ref. 10)	0.59 (Ref. 50)	0.44
	0.59 (Ref. 9)		0.59 (Ref. 10)	
r_H^{exp} (Å)	0.59 (Ref. 54)		0.59 (Ref. 53)	0.47

faces of Ni, Rh, and Pd are characterized by hollow site occupation at monolayer coverage.

In Table IV we contrast calculated and measured energies and hydrogen radii—as determined from the calculated and measured adsorption heights or bond lengths—with those of H/Ir(100) of our present investigation (we leave out results of a DFT calculation which used the local density approximation[55]). For the 3*d* (Ni) over 4*d* (Rh, Pd) to 5*d* (Ir) metals there is increasing competition between hollow and bridge sites. While for Ni the hollow site is leading by a relative wide margin [193 meV,[8] 256 meV (Ref. 9)] with respect to the bridge site, the lead is only by 85 meV for Rh (Ref. 10) and by 120 meV for Pd.[11] Also, in all these cases the top site is by far the most unfavorable site (also reported in Ref. 55). Yet, for the (100) surface of the 5*d* metal Ir the situation is completely different: Now the bridge site is clearly the most favorable position *and* the hollow site is the most unfavorable one (with the top site lying in between the two). The reader should also note that, except for Pd, the experimental values as determined by TDS are all lower than the calculated ones indicative for overbinding effects in the calculations as discussed above. One might suspect the exception for Pd is due to the existence of some (small) activation energy, yet none has been found in quantum dynamics investigations.[56] All the mentioned adsorption systems have in common is that there is almost no coverage dependence of the adsorption energies as long as the adsorption site remains the same. Compared to the clean (100) surfaces of Ni, Rh, and Pd we find a relatively strong and oscillatory multilayer relaxation for clean Ir(100). As expected hydrogen adsorption weakens the contractions or expansions of substrate layer spacings. So, there is still a contraction of the top spacing (followed by a small expansion), but its value is reduced due to the bonding influence of the adsorbate as also observed in a large number of other cases.[45]

The different binding situation of hydrogen on the (100) surface of Ir compared to the surfaces of Ir, Rh, and Pd is also reflected by the covalent radii r_H of hydrogen which we calculated from the adsorption heights or bond lengths using the experimental and calculated covalent radii of the transition metals (experimental values: Ni: 1.24 Å, Rh: 1.34 Å, Pd: 1.37 Å, Ir: 1.36 Å). As displayed in Table IV the experimentally determined and computed values for Ni, Rh, and Pd, i.e., for hollow site adsorption, are all close to $r_H \approx 0.6$ Å, while that for bridge site adsorption on Ir is definitely $r_H < 0.5$ Å. This reduced value for bridge site occupation is in line with a recent investigation of H adsorption on the strongly anisotropic, missing-row reconstructed Pt(110) surface[57] in which bridge sites have been found, too. The DFT calculated hydrogen radius in this phase is $r_H = 0.39$ Å.[58] The authors argue that the bridge site occupation is due to a directional bond formation with Pt *d* orbitals which are expanded due to the relativistic contraction of the *s* orbitals. This scenario is likely to hold also in the present case and must be much different from the case of fcc(100) surfaces of the 3*d* and 4*d* metals. We also mention that no bridge sites but quasithreefold coordinated sites have been found for the (unreconstructed) (110) surfaces of Ni,[8] Rh,[47] and Pd.[50]

In conclusion we have found that the structure and energetics of hydrogen adsorption on Ir(100)-(1×1) is significantly different from that on 3*d* and 4*d* fcc(100) metal surfaces. This seems to be due to the different electronic structure of the substrate and should most likely hold for Pt also. In the present case the detailed determination of the adsorption scenario, i.e., coverage *and* adatom sites, was only possible by the *combined* application of DFT and quantitative LEED.

*Corresponding author. Fax: +49-9131-8528400. Electronic mail: klaus.heinz@physik.uni-erlangen.de

[1] L. Hammer, W. Meier, A. Klein, P. Landfried, A. Schmidt, and K. Heinz, Phys. Rev. Lett. **91**, 156101 (2003).
[2] J. Küppers and H. Michel, Appl. Surf. Sci. **3**, 179 (1979).
[3] K. Heinz, G. Schmidt, L. Hammer, and K. Müller, Phys. Rev. B **32**, 6214 (1985).
[4] W. Meyer, A. Klein, L. Hammer, and K. Heinz, Phys. Rev. B (to be published).
[5] J. K. Nørskov, J. Chem. Phys. **90**, 7461 (1989).
[6] S. E. Wonchoba and D. G. Truhlar, Phys. Rev. B **53**, 11222 (1996).
[7] T. R. Mattson, G. Wahnstrom, L. Bengtsson, and B. Hammer, Phys. Rev. B **56**, 2258 (1997).
[8] G. Kresse and J. Hafner, Surf. Sci. **459**, 287 (2000).
[9] B. Bathia and D. S. Sholl, J. Chem. Phys. **122**, 204707 (2005).
[10] A. Eichler, J. Hafner, and G. Kresse, J. Phys.: Condens. Matter **8**, 7659 (1996).
[11] G. Pauer, A. Eichler, M. Sock, M. Ramsey, F. Netzer, and A. Winkler, J. Chem. Phys. **119**, 1 (2003).
[12] C. Klein, A. Eichler, E. L. D. Hebenstreit, G. Pauer, R. Koller, A. Winkler, M. Schmid, and P. Varga, Phys. Rev. Lett. **90**, 176101 (2003).
[13] P. E. Blöchl, Phys. Rev. B **50**, 17953 (1994).
[14] G. Kresse and D. Joubert, Phys. Rev. B **59**, 1758 (1999).
[15] G. Kresse and J. Hafner, Phys. Rev. B **47**, R558 (1993).
[16] G. Kresse and J. Hafner, J. Phys.: Condens. Matter **6**, 8245 (1994).
[17] G. Kresse and J. Furthmüller, Phys. Rev. B **54**, 11169 (1996).
[18] J. P. Perdew, J. A. Chevary, S. H. Vosko, K. A. Jackson, M. R. Pederson, D. J. Singh, and C. Fiolhais, Phys. Rev. B **46**, 6671 (1992).
[19] D. E. Gray, *American Institute of Physics Handbook*, 7th ed. (McGraw-Hill, New York, 1972).
[20] C. Kittel, *Introduction to Solid State Physics*, 7th ed. (Wiley, New York, 1996).
[21] J. P. Perdew, K. Burke, and M. Ernzerhof, Phys. Rev. Lett. **77**, 3865 (1996).
[22] E. Wimmer, H. Krakauer, M. Weinert, and A. J. Freeman, Phys. Rev. B **24**, 864 (1981).
[23] M. Weinert, J. Math. Phys. **22**, 2433 (1981).
[24] M. Weinert, E. Wimmer, and A. J. Freeman, Phys. Rev. B **26**, 4571 (1982).
[25] P. J. Rous, J. B. Pendry, D. K. Saldin, K. Heinz, K. Müller, and N. Bickel, Phys. Rev. Lett. **57**, 2951 (1986).
[26] P. J. Rous, Prog. Surf. Sci. **39**, 3 (1992).
[27] K. Heinz, Rep. Prog. Phys. **58**, 637 (1995).
[28] V. Blum and K. Heinz, Comput. Phys. Commun. **134**, 392 (2001).
[29] J. Rundgren, Phys. Rev. B **68**, 125405 (2003).
[30] M. Kottcke and K. Heinz, Surf. Sci. **376**, 352 (1997).
[31] J. B. Pendry, J. Phys. C **13**, 937 (1980).
[32] A. Schmidt, W. Meier, L. Hammer, and K. Heinz, J. Phys.: Condens. Matter **14**, 12353 (2002).
[33] K. Heinz and L. Hammer, Z. Kristallogr. **213**, 615 (1998).
[34] K. Johnson, Q. Ge, S. Titmuss, and D. A. King, J. Chem. Phys. **112**, 10460 (2000).
[35] J. P. Perdew, J. A. Chevary, S. A. Vosko, K. A. Jackson, M. R. Pederson, D. J. Singh, and C. Fiolhais, Phys. Rev. B **48**, 4978(E) (1993).
[36] C. Filippi, D. J. Singh, and C. J. Umrigar, Phys. Rev. B **50**, 14947 (1994).
[37] C. Stampfl, H. J. Kreuzer, S. H. Payne, H. Pfnür, and M. Scheffler, Phys. Rev. Lett. **83**, 2993 (1999).
[38] B. Hammer, L. B. Hansen, and J. K. Nørskov, Phys. Rev. B **59**, 7413 (1999).
[39] Y. Zhang and W. Yang, Phys. Rev. Lett. **80**, 890 (1998).
[40] K. P. Huber, in *American Institute of Physics Handbook*, edited by E. D. Gray (McGraw-Hill, New York, 1972).
[41] D. Tománek, S. Wilke, and M. Scheffler, Phys. Rev. Lett. **79**, 1329 (1997).
[42] P. A. Redhead, Vacuum **12**, 203 (1962).
[43] D. A. King, T. M. Madey, and J. T. J. Yates, J. Chem. Phys. **55**, 3236 (1971).
[44] D. A. King, Surf. Sci. **47**, 384 (1975).
[45] P. R. Watson, M. A. Van Hove, and K. Hermann, *Surface Structure Data Base, Ver. 5.0* (National Institute of Standards and Technology, Gaithersburg, MD, 2004).
[46] K. Heinz and L. Hammer, Z. Phys. Chem. **197**, 173 (1996).
[47] W. Nichtl-Pecher, W. Oed, H. Landskron, K. Heinz, and K. Müller, Vacuum **41**, 297 (1990).
[48] N. Nishijima, H. Okuyama, N. Okuyama, T. Aruga, and W. Brenig, Surf. Sci. Rep. **57**, 113 (2005).
[49] H. Okuyama, M. Z. Hossain, T. Aruga, and M. Nishijima, Phys. Rev. B **66**, 235411 (2002).
[50] W. Dong, V. Ledentu, P. Sautet, E. Eichler, and J. Hafner, Surf. Sci. **411**, 123 (1998).
[51] K. Christmann, O. Schober, G. Ertl, and N. Neumann, J. Chem. Phys. **60**, 4528 (1974).
[52] L. J. Richter and W. Ho, J. Vac. Sci. Technol. A **5**, 453 (1987).
[53] F. Besenbacher, I. Stensgaard, and K. Martensen, *The Structure of Surfaces II*, Springer Series Surface Sciences (Springer, Berlin, 1988), Vol. 11, p. 195.
[54] I. Stensgaard and F. Jakobsen, Phys. Rev. Lett. **54**, 711 (1985).
[55] S. Wilke, D. Hennig, and R. Löber, Phys. Rev. B **50**, 2548 (1994).
[56] A. Gross, S. Wilke, and M. Scheffler, Phys. Rev. Lett. **75**, 2718 (1995).
[57] Z. Zhang, M. Minca, C. Deisl, T. Loerting, A. Menzel, E. Bertel, R. Zucca, and J. Redinger, Phys. Rev. B **70**, 121401(R) (2004).
[58] J. Redinger (private communication).